UC Santa Cruz
UC Santa Cruz Previously Published Works

Title

Origin of enhanced anisotropy in FePt-C granular films revealed by XMCD

Permalink

https://escholarship.org/uc/item/93869768

Journal

Applied Physics Letters, 114(16)

ISSN

0003-6951

Authors

Streubel, Robert
N'Diaye, Alpha T
Srinivasan, Kumar
et al.

Publication Date

2019-04-22

DOI

10.1063/1.5092719

Peer reviewed

Origin of enhanced anisotropy in FePt-C granular films revealed by XMCD

Robert Streubel,[1, a)] Alpha T. N'Diaye,[2] Kumar Srinivasan,[3] Antony Ajan,[3] and Peter Fischer[1, 4]

[1)]*Materials Sciences Division, Lawrence Berkeley National Laboratory, Berkeley CA 94720, USA*

[2)]*Advanced Light Source, Lawrence Berkeley National Laboratory, Berkeley CA 94720, USA*

[3)]*Western Digital, San Jose CA 95131, USA*

[4)]*Physics Department, UC Santa Cruz, Santa Cruz CA 95064, USA*

We study the effect of carbon segregants on the spin and orbital moments of $L1_0$ FePt granular media and report an effective decoupling of the structural film properties from the magnetic parameters of the grains. Carbon concentration reduces the grain size from $(200 \pm 160)\,\mathrm{nm}^2$ down to $(50 \pm 20)\,\mathrm{nm}^2$ for 40 mol.%C, and improves sphericity and order of grains, while preserving crystalline order, spin and orbital moments, as well as perpendicular magnetocrystalline anisotropy. We identify the primary cause of enhanced saturation and coercive fields as the reduced demagnetization fields of individual grains. The ability to shrink grains without impairing their magnetic properties is a critical requirement for the commercialization of Heat-Assisted Magnetic Recording.

Hard-disk drives utilizing magnetic recording technology are the dominant auxiliary storage devices owing to capacity and price advantages. Within the next few years, magnetic recording technology is expected to transition from Perpendicular Magnetic Recording (PMR) to energy assisted technologies, such as Heat-Assisted Magnetic Recording (HAMR)[1]. For these applications, the $L1_0$ phase of FePt offering a very high magnetocrystalline anisotropy of $7\,\mathrm{MJ/m}^3$ is the material system of choice[2,3]. The high anisotropy allows for pushing the smallest thermally stable grain sizes down to $(3 \sim 4)\,\mathrm{nm}$, which corresponds to a storage density of several Tbits/in^2. The writing process has to be energy assisted to overcome the high anisotropy at room temperature, e.g. facilitating laser induced heating of the FePt media above its Curie temperature. Magnetically isolated granular FePt films are typically sputter deposited alongside other constituents that preferentially form grain boundary phases or segregants[3–7]. These constituents include carbon, oxides, nitrides and carbides. Aside from segregants, dopants such as Ag and Cu may be introduced into the FePt to control the structural ordering temperature, Curie temperature and other properties. A partial FePt/segregant phase separation can result in intermixing at the interface between the two. For instance, a core-shell type of microstructure with an FeO_x shell surrounding an FePt grain has been observed in FePt-SiO$_2$ systems[8]. While it is well understood that segregants and dopants in the FePt system strongly influence the magnetic bit recording parameters[3–7], little is known about their effect on spin and orbital moments, and demagnetization field contributions.

In this work, we investigate the effect of carbon segregants on the spin and orbital Fe moments of $L1_0$ FePt nanogranular media, and determine the relation of enhanced coercive and saturation fields to the grain size.

The spin and orbital moments are quantified with x-ray absorption spectroscopy (XAS) and x-ray magnetic circular dichroism (XMCD) spectroscopy. The carbon promotes sphericity and a narrow size distribution of the magnetic grains, which increase saturation and coercive fields due to reduced demagnetization fields, while preserving spin and orbital moments, and perpendicu-
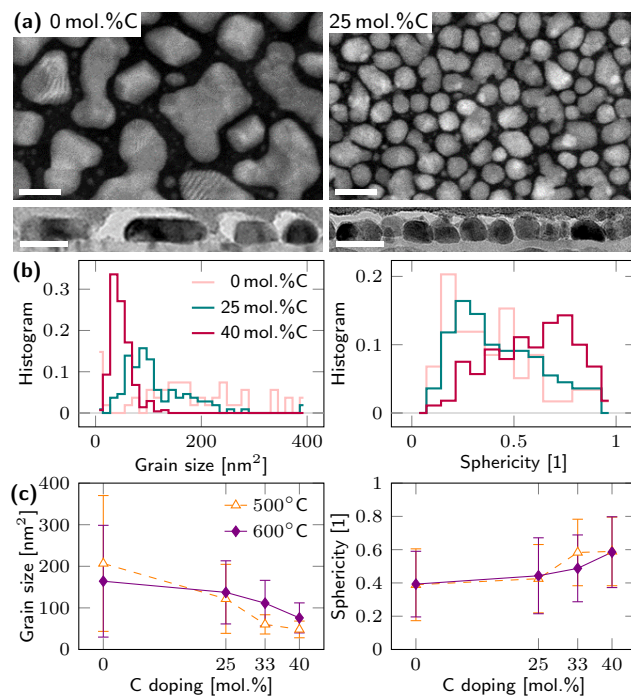

FIG. 1. Structural modification of $L1_0$ FePt granular microstructures by addition of carbon segregants. (a) Top and cross-sectional view of 10 nm-thick FePt film grown at 600°C recorded in STEM-mode and bright-field mode of TEM, respectively. Scale bars are 20 nm. (b) Distribution of grain size and sphericity quantifying transformation from large, irregular to small, circular grains. (c) Mean values of the grain size and shape for different growth temperatures.

a)Electronic mail: streubel@lbl.gov

lar magnetocrystalline anisotropy. The FePt films were prepared at Western Digital following the procedure described in Ref.[8]. We note in particular: (1) The FePt-C films were deposited by co-sputtering from separate FePt and C targets. Three sets of 5 nm-thick films were grown in-situ at 400°C, 500°C and 600°C substrate temperatures. We additionally grew 10 nm-thick sister samples to minimize experimental uncertainty of crystallographic analysis. (2) We use a 4 nm-thick Co capping layer deposited at room temperature to facilitate the complete reversal of the moments during the XAS/XMCD experiments. Without the Co capping layer, the switching fields for the ordered FePt films in this study are well beyond 30 kOe and experimentally not accessible. The Co layer solely serves as a switching-assist layer, so that the samples can be saturated in the experimentally accessible fields, and affects neither morphology nor magnetic properties of the FePt-C system.

The structural properties of the granular films without Co capping layer are probed using scanning electron microscopy with in-lens and electron backscatter detector (EBSD) as well as scanning transmission electron microscopy and bright-field transmission electron microscopy of top and cross-sectional view, respectively. Each sample represents a discontinuous, granular film as exemplarily shown for specimens grown at 500°C [Fig. 1(a)]. The grain morphology is quantified by the distribution of grain size and shape (sphericity) [Fig. 1(b)], which reveal a systematic linear decrease (increase) in grain size (sphericity) with increasing carbon concentration. In particular, the grain size of FePt is reduced from $(200 \pm 160)\,\mathrm{nm}^2$ down to $(50 \pm 20)\,\mathrm{nm}^2$ for 40 mol.%C concentration [Fig. 1(c)]. Note that these values may vary with FePt film thickness. The experimental uncertainty is given by the standard deviation of the corresponding distributions. The sphericity is declared as the ratio of the two major axes of individual grains approximated as ellipses. While specimens grown at 500°C and 600°C behave qualitatively similarly in view of film morphology [Fig. 1(c)], a growth temperature of 400°C leads to a maze microstructure which prevails for carbon concentrations up to 40 mol.%.

The carbon driven morphology change preserves the crystalline structure, oriented perpendicularly to the surface, for concentrations up to 40 mol.% (30 vol.%) [Fig. 2(a)] as evident from a nearly constant rocking curve width of $(6.2 \pm 0.2)°$, and improves the overall surface roughness from 1.2 nm (0 mol.%C) to 0.6 nm (> 25 mol.%C). However, it strongly affects saturation field and coercivity, which increases from 0 to 33 mol.%C [Fig. 2]. The decrease in coercivity at 40 mol.%C is similar to the (002) peak intensity. Interestingly, the relative change of both fields as a function of carbon concentration is similar for different measurement temperatures and particularly growth temperatures despite distinct values for FePt with 0 mol.%C. This behavior suggests a governing role of extrinsic properties, i.e. grain morphology, not crystallinity, as discussed in detail be-
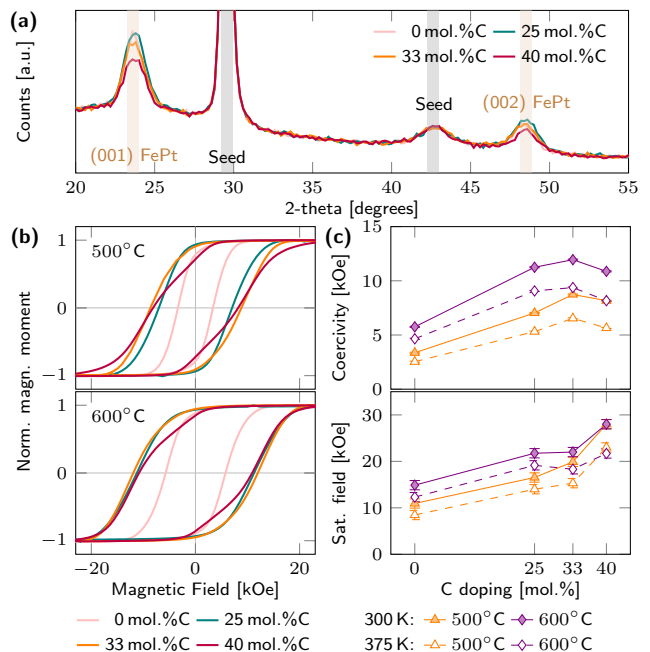
FIG. 2. Preservation of crystallinity and enhancement of coercive and saturation fields along the easy axis with increasing carbon concentration. (a) Two-theta x-ray diffraction scans of 10 nm-thick FePt film confirming crystallographic properties of $L1_0$ FePt. (b) Room temperature out-of-plane magnetic hysteresis loops recorded by a Physical Property Measurement System. (c) Coercive and saturation fields of samples deposited at 500°C and 600°C, measured at 300 K and 375 K.

low. The dependence on growth temperature originates from a slightly better crystalline ordering for specimens deposited at 600°C. The percentage of switched grains in specimens with 40 mol.%C at remanence is similar to that of pure FePt of roughly 10%. Note that the lack of a fully saturated remanent state and relatively low coercive/saturation fields (thrice less with Co capping) are due to the exchange-spring reversal caused by coupling to the Co capping layer. A similar carbon concentration dependence of the coercive field peaking at 30 mol.% was observed in previous works and assigned to an improved crystallinity[3,4].

Further insight into chemical and magnetic properties is given by XAS and XMCD spectroscopy performed at beamline 6.3.1 at the Advanced Light Source, and quantifying spin and orbital moments to assess the governing magnetocrystalline anisotropy. The XAS near the Fe $L_{3,2}$ edges [(690 ~ 750) eV] are recorded in the presence of an external magnetic field (± 19 kOe) normal to the sample surface. The spectra plotted in Figure 3(a) are typical for metallic FePt, and confirm that carbon solely affects the film morphology but not the chemistry as it migrates to the grain boundaries instead of intercalation. For comparison, FePt specimens with 50 mol.%C reveal an obvious shoulder of the L_3 absorption peak associated with Fe-C hybridization and a car-
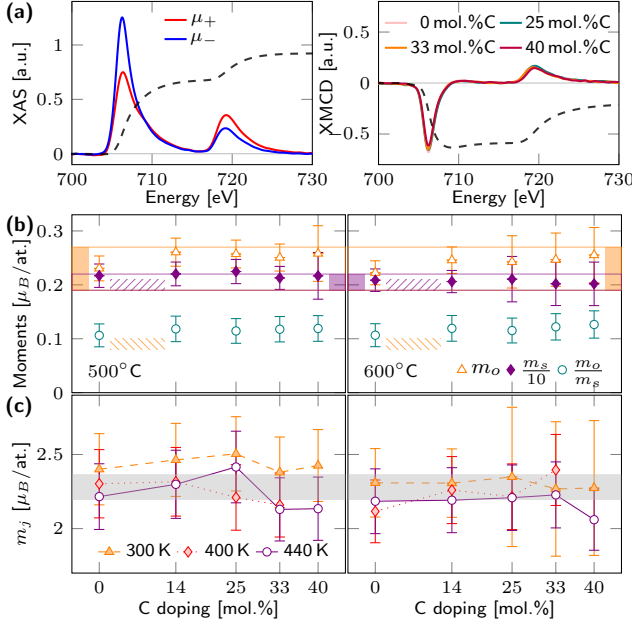
FIG. 3. Quantification of spin and orbital moments utilizing x-ray magnetic circular dichroism spectroscopy. (a) X-ray absorption spectra and XMCD signal near Fe $L_{3,2}$ edges shown for $L1_0$ FePt grown at 500°C and saturated out-of-plane in ±19 kOe. Dashed lines plot the integrals used for quantitative analysis as defined in the text. (b) Room temperature spin and orbital moments as well as their ratio as a function of carbon concentration. Colored horizontal lines indicate literature values for Fe moments in $L1_0$ FePt. Striped lines refer to bcc Fe moments. (c) Total moments plotted for various measurement temperatures and carbon concentration.
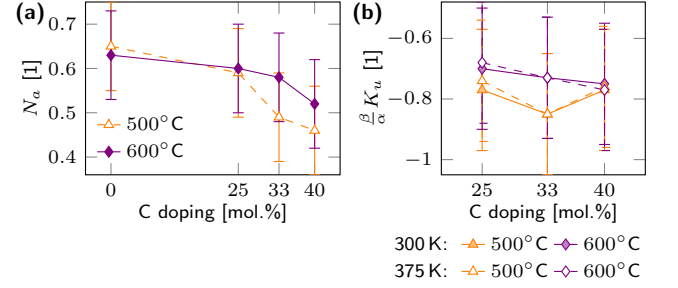

FIG. 4. Indirect confirmation of dominant role of shape anisotropy. (a) Normal component of demagnetization tensor estimated for rotation ellipsoid approximation. (b) Normalized magnetocrystalline anisotropy with nearly constant values indicating governing role of shape anisotropy.

bon inercalation. Despite the high sensitivity of XAS to chemical bonding, it is impossible to completely exclude hybridization at 40 mol.%C; However, it does not impact the magnetic moments. This interpretation is consistent with micromagnetic simulations of the effect of intercalated carbon inside $L1_0$ FePt that leads to a fading of magnetocrystalline anisotropy at 10 mol.%C and beyond[3]. Calculating the integrals of both XAS and XMCD spectra $r = \int_{L_3+L_2} (\mu_+ + \mu_-)\, d\omega$, $q = \int_{L_3+L_2} (\mu_+ - \mu_-)\, d\omega$, $p = \int_{L_3} (\mu_+ - \mu_-)\, d\omega$, shown as dashed curves in Figure 3(a), allows for quantifying the orbital and spin moment using the sum rules[9,10] according to $m_o = -\frac{4q}{3r} n_h$ and $m_s = -\frac{6p-4q}{r} n_h \left(1 + \frac{7\langle T_z \rangle}{2\langle S_z \rangle}\right)^{-1}$, respectively. The Fe electron hole density is set to $n_h = 3.73$ according to first-principle calculations[11]. Note that the expectation value of the magnetic dipole operator $\langle T_z \rangle$ is constant for all investigated systems because of identical film thicknesses. Additionally, the $L1_0$ crystal structure of FePt causes a substantial normal spin-orbit coupling that nullifies surface contributions. Hence, contributions from the magnetic dipole operator are neglected to simplify the study of the impact of carbon concentration. The accordingly obtained data reveal sig-

nificantly larger orbital moments compared with bcc Fe[12] due to spin-orbit coupling with adjacent Pt layers, and similar values for spin moments [Fig. 3(b)]. In fact, the experimental data agree well with the range of moments reported in previous works on $L1_0$ FePt and $L1_0$ FePt-C[3,7,13,14]. Overall, the spin moment is within experimental uncertainty unaffected by the carbon concentration affirming the absence of chemical disorder or a deadlayer surrounding each grain. The slightly increased orbital moment, virtually the same for any investigated carbon concentration, indicates an enhanced vertical ordering of the Pt/Fe layer system compared with pure $L1_0$ FePt, that does not further improve with carbon concentration. For specimens grown at 600°C, the saturation field even with the Co capping layer exceeds at room temperature the experimentally accessible value of 19 kOe leading to a 90% saturated sample [Fig. 2]. This partial saturation is taken into account by scaling both orbital and spin moments, which induces a slightly larger uncertainty compared with other measurements. Furthermore, the strong spin-orbit coupling and corresponding perpendicular magnetocrystalline anisotropy of the $L1_0$ FePt films suppress an obvious temperature dependence in the probed range (300 ∼ 440) K [Fig. 3(c)]. Note that both statements on carbon concentration and temperature apply analoguously to the magnetocrystalline anisotropy due to its direct relation to the ordering of orbital moments.

Consequently, the enhancement of coercive and saturation fields has to originate from the change in grain morphology. To confirm this assertion, we compare the contributions of demagnetization and magnetocrystalline anisotropy energy to the overall energy. The anisotropy energy E associated with the switching of a magnetic grain can be calculated via $E = \mu_0 \int_{e.a.} M\, dH - \mu_0 \int_{h.a.} M\, dH$ of hysteresis-free curves along the easy and hard axis. Note that the significant magnetocrystalline anisotropy of the $L1_0$ FePt film does not allow for saturating the film along the hard axis. Hence, we approximated the relative change of the energy E as a function of grain size (carbon concentration) from the

easy axis hysteresis loops as $E \approx \frac{1}{2}\mu_0 M_s H_s$ assuming a similar relative change for saturation fields H_s along hard and easy axis. Furthermore, the magnetic energy $E \approx E_d + E_u$ comprises demagnetization energy $E_d = \frac{1}{2}\mu_0 M_s^2 V \mathbf{m^T N m} \approx \alpha N_a$ and the magnetocrystalline anisotropy energy $E_u = \beta K_u$, favoring easy plane and easy axis anisotropy, respectively. Here, $\mathbf{m}$ is the unit magnetization vector taking the value $(0,0,1)$ for perpendicularly magnetized grains, and $\mathbf{N}$ is the demagnetization tensor. The corresponding demagnetization factor N_a perpendicular to the substrate surface is defined by $N_a = \frac{1}{2}abc \int_0^\infty \frac{\mathrm{d}x}{(a^2+x)\sqrt{(a^2+x)(b^2+x)(c^2+x)}}$ with major axes a, b and c[15]. In this notation, a is equal to half the film thickness ($2.5\,\mathrm{nm}$). The grains are approximated as rotation ellipsoids with a circular lateral expansion ($b = c = \sqrt{A/\pi}$), which slightly underestimates N_a for large grains. The grain size A is taken from Fig. 1(c). The coefficients α and β denote quantities, i.e. volume V and saturation magnetization M_s, which are in first approximation constant throughout the sample series and therefore irrelevant to the following estimation. As evident from Figure 4(a), the carbon concentration of the $5\,\mathrm{nm}$-thick films significantly alters the demagnetization field owing to a shrinking of the grains down to nearly isotropic expansion. The increasingly relevant demagnetization factor combined with the grain size distribution explains why the slope of the hysteresis becomes more shallow at large carbon concentrations [Fig. 2(a)]. The demagnetization field contribution governs the relative change of the saturation fields with respect to pure FePt

$$\frac{H_s^j}{H_s^0} \approx \frac{\alpha N_a^j + \beta K_u}{\alpha N_a^0 + \beta K_u},$$

which is confirmed by calculating $\frac{\beta}{\alpha}K_u$ [Fig. 4(b)]. Note that the sole purpose of this estimate is to verify or refute a carbon dependence of the normalized anisotropy $\frac{\beta}{\alpha}K_u$ after subtracting contributions of grain size dependent demagnetization fields. It does not serve as a quantification of the anisotropy itself. The negative sign is caused by counteracting magnetocrystalline and demagnetization field favoring easy axis and easy plane anisotropy, respectively. Within experimental uncertainty, primarily originating from the relatively broad grain size distribution [Fig. 1(c)] and underestimated demagnetization fields for large grains, all samples reveal the same $\frac{\beta}{\alpha}K_u$ value indicating a modification of the magnetic properties primarily driven by the grain morphology. This result implies that the current understanding of the role of carbon, enhancing coercivity and anisotropy due to improved crystallinity and hence magnetocrystalline anisotropy, is by itself insufficient.

In conclusion, we showed that carbon concentration of $L1_0$ FePt granular microstructures significantly improves structural properties: it promotes sphericity and a narrow size distribution of the magnetic grains. This microstructure supports enhanced saturation and coercive fields due to reduced demagnetization fields,

while preserving, up to $40\,\mathrm{mol.\%C}$, spin and orbital moments, and perpendicular magnetocrystalline anisotropy. Higher carbon concentrations cause intercalation impairing structural and magnetic quality. While specimens grown at 500°C show a more prominent structural change compared with 600°C, the latter exhibit larger saturation and coercive field values due to superior crystalline order. In contrast, 400°C growth temperature leads to a maze microstructure. We found that carbon segregates at the grain boundaries, thereby reducing in the present case of $5\,\mathrm{nm}$-tick $L1_0$ FePt the grain size from $(200 \pm 160)\,\mathrm{nm}^2$ down to $(50 \pm 20)\,\mathrm{nm}^2$. The accordingly altered demagnetization field of individual grains is the primary cause of an increased effective perpendicular magnetic anisotropy in contrast to the current understanding of an improved crystallinity and magnetocrystalline anisotropy.

[1]D. Weller, G. Parker, O. Mosendz, E. Champion, B. Stipe, X. Wang, T. Klemmer, G. Ju, and A. Ajan, IEEE Trans. Magn. **50**, 1 (2014).

[2]D. Weller, O. Mosendz, G. Parker, S. Pisana, and T. S. Santos, Phys. Status Solidi A **210**, 1245 (2013).

[3]J. Wang, H. Sepehri-Amin, H. Tajiri, T. Nakamura, K. Masuda, Y. Takahashi, T. Ina, T. Uruga, I. Suzuki, Y. Miura, and K. Hono, Acta Mater. **166**, 413 (2019).

[4]A. Perumal, Y. K. Takahashi, and K. Hono, J. Appl. Phys. **105**, 07B732 (2009).

[5]J. Chen, J. Hu, B. Lim, Y. Ding, G. Chow, and G. Ju, IEEE Trans. Magn. **45**, 839 (2009).

[6]S. Pisana, O. Mosendz, G. J. Parker, J. W. Reiner, T. S. Santos, A. T. McCallum, H. J. Richter, and D. Weller, J. Appl. Phys. **113**, 043910 (2013).

[7]S. Sakamoto, K. Srinivasan, R. Zhang, O. Krupin, K. Ikeda, G. Shibata, Y. Nonaka, Z. Chi, M. Sakamaki, K. Amemiya, A. Fujimori, and A. Ajan, Phys. Rev. B **96**, 144437 (2017).

[8]Y. Zhang, A. Kalitsov, J. Ciston, O. Mryasov, B. Ozdol, J. Zhu, S. Jain, B. Zhang, B. Livshitz, A. Chernyshov, A. Ajan, P. Dorsey, G. Bertero, R. Acharya, A. Greene, and S. Myers, AIP Advances **8**, 125018 (2018).

[9]B. T. Thole, P. Carra, F. Sette, and G. van der Laan, Phys. Rev. Lett. **68**, 1943 (1992).

[10]P. Carra, B. T. Thole, M. Altarelli, and X. Wang, Phys. Rev. Lett. **70**, 694 (1993).

[11]S. Miwa, M. Suzuki, M. Tsujikawa, K. Matsuda, T. Nozaki, K. Tanaka, T. Tsukahara, K. Nawaoka, M. Goto, Y. Kotani, T. Ohkubo, F. Bonell, E. Tamura, K. Hono, T. Nakamura, M. Shirai, S. Yuasa, and Y. Suzuki, Nat. Commun. **8**, 15848 (2017).

[12]C. T. Chen, Y. U. Idzerda, H.-J. Lin, N. V. Smith, G. Meigs, E. Chaban, G. H. Ho, E. Pellegrin, and F. Sette, Phys. Rev. Lett. **75**, 152 (1995).

[13]O. Dmitrieva, M. Spasova, C. Antoniak, M. Acet, G. Dumpich, J. Kästner, M. Farle, K. Fauth, U. Wiedwald, H.-G. Boyen, and P. Ziemann, Phys. Rev. B **76**, 064414 (2007).

[14]D. Xu, C. Sun, J. Chen, S. Heald, B. Sanyal, R. Rosenberg, T. Zhou, and G. Chow, J. Phys. D: Appl. Phys. **48**, 255001 (2015).

[15]A. Hubert and R. Schäfer, *Magnetic Domains* (Springer, 1998).